COMPUTER METHODS IN BIOMECHANICS AND BIOMEDICAL ENGINEERING
2019, VOL. 22, NO. 14, 1144–1152
https://doi.org/10.1080/10255842.2019.1644503

Taylor & Francis
Taylor & Francis Group

Check for updates

Repeatability, reproducibility, and agreement of three computational methods to approximate the functional flexion-extension axis of the tibiofemoral joint using 3D bone models of the femur

Rocio Lozano[a], Stephen M. Howell[a] and Maury L. Hull[a,b,c]

[a]Department of Biomedical Engineering, University of California, Davis, Davis, CA, USA; [b]Department of Mechanical Engineering, University of California, Davis, Davis, CA, USA; [c]Department of Orthopaedic Surgery, University of California, Davis Medical Center, Sacramento, CA, USA

ABSTRACT

Background: Closely approximating the functional flexion-extension (FE) axis of the tibiofemoral joint in 3D models of the femur is important when computing joint motions which are physiologic. The objectives were to 1) develop methods to approximate the functional FE axis based on fitting circles, a tapered cylinder, and spheres to the posterior condyles, 2) determine the repeatability and reproducibility of each method, and 3) determine limits of agreement between pairs of axes.

Methods: For each method, the respective axis was determined in forty 3D bone models of the distal femur. Varus-valgus angles and internal-external axial angles were computed relative to standard planes.

Results: Repeatability and reproducibility were comparable for the tapered cylinder-based and sphere-based methods and better than that for the circle-based method. Limits of agreement were tightest when comparing the sphere-based and tapered cylinder-based axes. However, limits of agreement for the internal-external axial angle were wide at $+3.6^\circ$ to -3.9° whereas limits of agreement were tighter at $+1.4^\circ$ to -0.7° for the varus-valgus angle.

Conclusion: The tapered cylinder-based and sphere-based methods offer advantages of better repeatability and reproducibility over the circle-based method. However, the sphere-based and tapered cylinder-based axes are not interchangeable owing to wide limits of agreement for the internal-external axial angle. The tapered cylinder-based axis is preferred intuitively over the sphere-based axis because the spheres require fitting in both the sagittal and coronal planes whereas the tapered cylinder requires fitting in the sagittal plane only which is the plane of motion in flexion-extension.

ARTICLE HISTORY
Received 15 April 2019
Accepted 13 July 2019

KEYWORDS
Human knee; kinematics; total knee arthroplasty; Bland-Altman plot; interobserver; intraobserver

Introduction

Three-dimensional bone models have a variety of uses one of which is to quantify relative rigid body motions between the tibia and femur during passive flexion and weight bearing activities. Various methods have been used to measure relative rigid body motions and include single-plane and bi-plane fluoroscopy studies as well as motion tracking in cadaveric studies using various means. Regardless of the method used, coordinate systems must be specified for both the femur and the tibia to quantify the motions. For the relative rigid body motions to be clinically informative, the joint coordinate system of Grood and Suntay (Grood and Suntay 1983), which was recommended by the ISB (Wu et al. 2002), should be used. This joint coordinate system entails the use of three axes, one attached to the femur about which flexion-extension (FE) occurs, one attached to the tibia about which internal-external (IE) rotation occurs, and a floating axis mutually perpendicular about which varus-valgus (VV) rotation occurs. Medial-lateral (ML) translation occurs along the FE axis, anterior-posterior (AP) translation occurs along the VV axis, and compression-distraction (CD) occurs along the IE axis.

To establish the joint coordinate system of Grood and Suntay (Grood and Suntay 1983), the axes must be determined in the respective bones and, for the six degree-of-freedom motions to be physiologic, the axes specified must be the functional axes (i.e. axes about which the rotations actually occur). If the axes specified are other than the functional axes, then kinematic crosstalk will result (Piazza and Cavanagh 2000;

CONTACT Maury L. Hull mlhull@ucdavis.edu
© 2019 Informa UK Limited, trading as Taylor & Francis Group

Freeman 2001; McPherson et al. 2005) and the resulting motions will not be physiologic. Restricting attention to the femur and the functional FE axis, previous research has established that the functional FE axis is fixed in the femur during both passive motion (Hollister et al. 1993; Eckhoff et al. 2003, 2005) and weight bearing motion (Churchill et al. 1998).

Recognizing that the functional FE axis is fixed in the femur, various methods have been used to approximate this axis in 3D bone models of the femur. These methods include fitting circles to projections of the medial and lateral femoral condyles on the sagittal plane and connecting the centers of these circles (Asano et al. 2001; Coughlin et al. 2003), fitting a cylinder to the posterior regions of the femoral condyles (Moro-oka et al. 2008; Matsuki et al. 2017), and fitting spheres to the femoral condyles (Kurosawa et al. 1985; Wilson et al. 2000; Victor et al. 2009).

To assess the efficacy of any method used to approximate the functional FE axis, two important metrics are repeatibility and reproducibility (National Institute of Standards and Technology 2007; Bartlett and Frost 2008). Since confusion exists surrounding the meaning and hence use of the terms in the literature, definitions of these metrics are appropriate. Repeatability refers to the variation in repeat measurements made on the same subject under identical conditions (National Institute of Standards and Technology 2007). Identical conditions require that measurements are made by the same instrument or method, the same observer (or rater) if human input is required, and over a short period of time during which the value of the dependent variable of interest is constant. Variability in measurements made on the same subject in a repeatability study can be ascribed only to errors due to the measurement process itself (Bartlett and Frost 2008). Reproducibility refers to the variation in measurements made on a subject under changing conditions (National Institute of Standards and Technology 2007). The changing conditions may be due to different measurement methods or instruments being used, different observers (or raters), or over a period of time during which the 'error free' value of the dependent variable of interest could undergo non-negligible change (Bartlett and Frost 2008). Although previous methods based on fitting circles, cylinders, and spheres have been used to approximate the functional FE axis, few studies have quantified the repeatability and reproducibity of the methods used. Moreover, the methods were not described with sufficient detail to enable their reproduction.

The objectives of the present study were threefold. The objectives were to 1) develop methods to approximate the functional FE axis based on fitting circles, a tapered cylinder, and spheres to the posterior condyles, 2) determine the repeatability and reproducibility of each method, and 3) determine the agreement between pairs of the axes generated by the three methods (i.e. circles vs. tapered cylinder; circles vs. spheres; spheres vs. tapered cylinder).

Methods

Forty, three-dimensional (3D) bone models of distal femurs from Caucasian patients (24 male, 16 female) were constructed from thin slice (0.7 mm (0.03 in)) 3.0 Tesla magnetic resonance images (MRI) randomly selected from the Osteoarthritis Initiative database (www.oai.ucsf.edu). Because these MR images were de-identified and publicly available, their use was not subject to institutional review board approval. The MR images were obtained as described in the Osteoarthritis Initiative protocol using the SAG 3D DESS WE series, which uses near anisotropic voxels (0.7 mm (0.03 in) slice thickness × 0.37 mm (0.01 in) × 0.46 mm (0.02 in)) to maximize in-plane sagittal spatial resolution in a reasonable acquisition time (10.5 min) (Peterfy et al. 2008). Prior to inclusion in the study, each MRI was viewed, and the knee was verified as not having any meniscal or ligament tears, evidence of arthritis in the form of subchondral wear, fracture, or hardware about the knee. Segmentation excluding the articular cartilage was performed with proprietary software developed to make models for patient-specific instrumentation (TechMah, LLC, Knoxville, TN, www.techmah.com). As a preliminary step to finding the axes using the methods described below, the 3D bone models were oriented in standard sagittal, axial, and coronal planes (Figure 1).

The circle-based and tapered cylinder-based axes were determined by first isolating the posterior condyles of the femur in several steps using Geomagic (3D Systems Design, Cary, NC) (Figure 2). Once isolated, 1 mm thick slices in the sagittal plane were created across each condyle and a circle was best-fit computationally to each slice using MATLAB (Figure 3). For the slice in each condyle with the largest radius circle, the centers of the circles were connected with a line to form the circle-based axis. Also a tapered cylinder was best-fit computationally for these two slices using the iterative closest point algorithm in Geomagic. The tapered cylinder-based axis was the axis of this tapered cylinder. Note that although the circles and the tapered

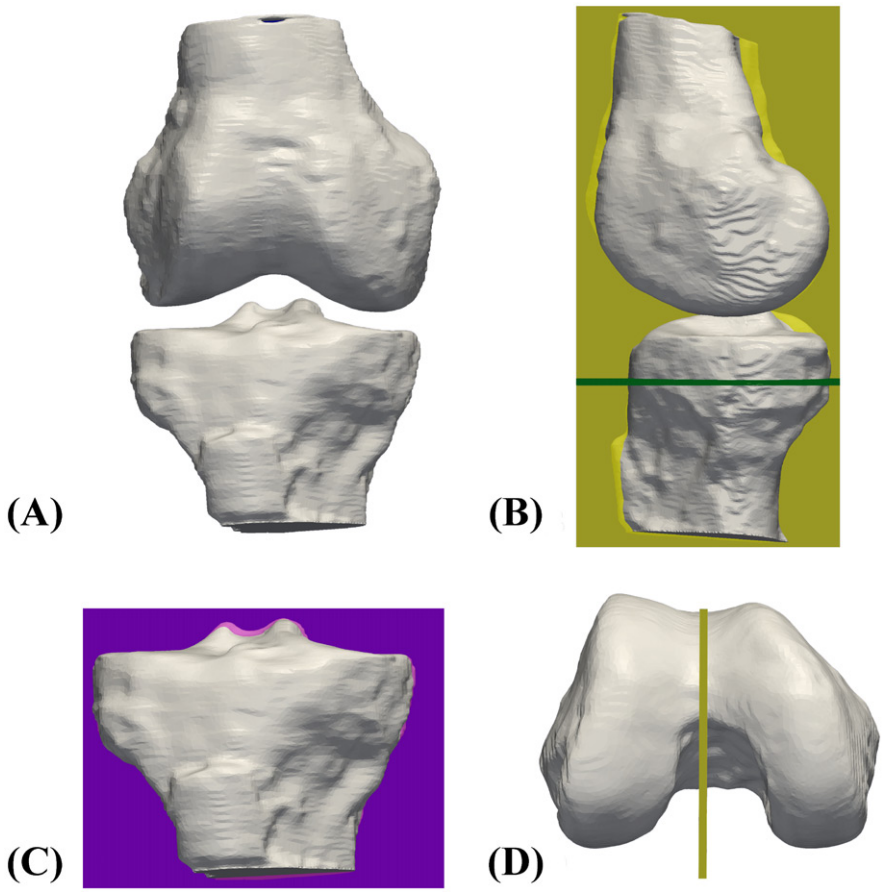

Figure 1. Standard planes. The composite shows a 3D model of a right knee sans patella and the steps for orienting the knee in the standard sagittal plane, the standard axial plane, and the standard coronal plane. (A) The bone model was imported into three-dimensional visualization software (Version 4.1.0 64-bit, Paraview, Kitware Inc., www.paraview.org). (B) The distal and posterior femoral condyles were superimposed to orient the femur and tibia in a standard sagittal plane (yellow). The standard axial plane (green) was oriented perpendicular to the standard sagittal plane and parallel to the medial articular surface of the tibial plateau. (C) The standard coronal plane (purple) was oriented mutually perpendicular to both the standard sagittal plane and the standard axial plane. (D) The line (yellow) on the distal surface of the femur is parallel to standard sagittal plane.

cylinder were fit to the same two slices, the resulting axes will necessarily differ because each circle was fit independently to the corresponding slice whereas the tapered cylinder was fit simultaneously to both slices.

The sphere-based axis was determined by first isolating the posterior condyles of the femur (Figure 2). Using an iterative closest point algorithm, Geomagic was used to best-fit two spheres, one to each isolated portion of the medial and lateral femoral condyles. The sphere-based axis connected the centers of the two spheres (Figure 4).

Data analyses

Three observers determined the corresponding axis using each of the methods on five 3D femur models repeated five times on each model in five analysis sessions with at least 48 hours between each session. Two angles were computed based on the standard planes. One was the varus-valgus angle determined as the angle between the projection of the axis on the standard coronal plane and the standard axial plane (Figure 5). The other was the internal-external axial angle determined as the angle between the projection of the axis on the standard axial plane and the standard sagittal plane (Figure 5).

The repeatability and reproducibility of the methods were quantified by computing the intraobserver and interobserver intraclass correlation coefficients (ICCs) using a two-factor analysis of variance (ANOVA) with random effects (Bartlett and Frost 2008). The first factor had three levels (observers 1, 2 and 3). The second factor had five levels (bone models 1 to 5). Two ANOVAs were performed, one for the varus-valgus angle and one for the internal-external axial angle. An ICC value of >0.9 indicates excellent agreement, 0.75

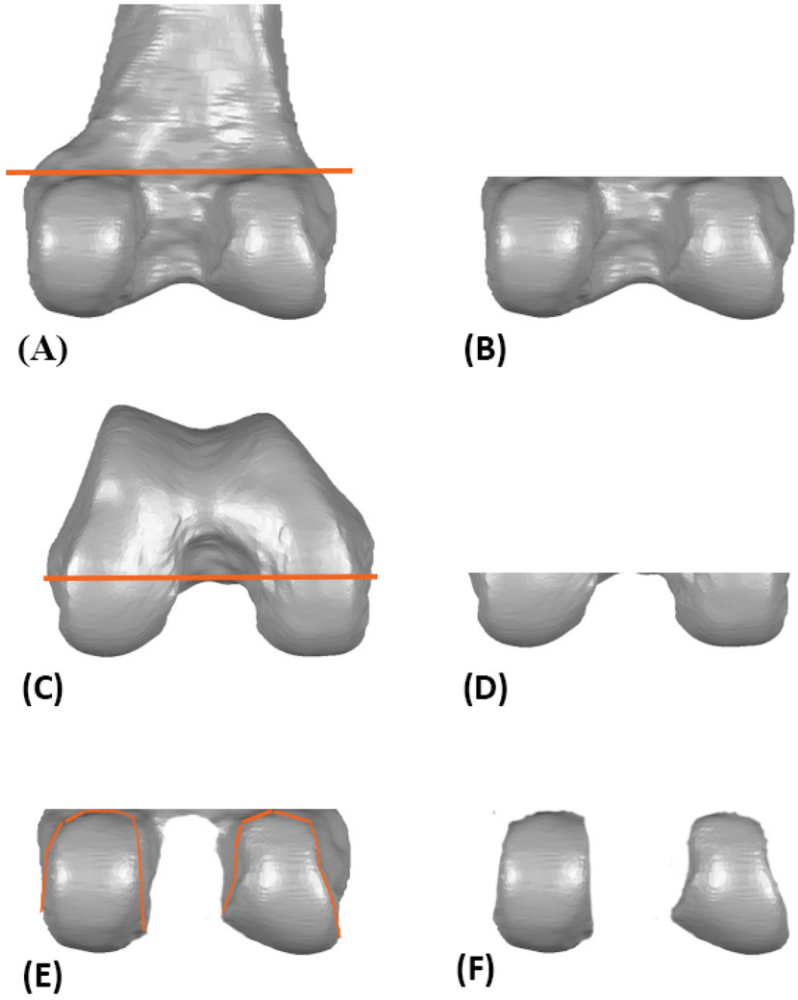

Figure 2. Process for isolating the posterior surfaces of the femoral condyles. The composite shows a 3D model of a right femur and the steps for isolating the posterior surfaces. (A) The femur was viewed in the standard coronal plane (posterior view) and a line tangent to the most medial and lateral proximal points of the limit of the articular cartilage was drawn. (B) All the bone proximal to that line was removed. (C) The femur was viewed in the standard axial plane (distal view) and a line tangent to the most posterior point on the notch was drawn. (D) All the bone anterior to that line was removed. (E) The femur was viewed in the standard coronal plane (posterior view). Outlines of the articular surfaces of the femoral condyles were drawn (F) All the bone outside of those lines was removed.

to 0.90 indicates good agreement, 0.5 to 0.75 indicates moderate agreement, and 0.25 to 0.5 indicates fair agreement (Indrayan 2013).

To quantify the agreement between pairs of methods, Bland-Altman plots were constructed and limits of agreement were determined (Bland and Altman 1986). These plots were constructed by computing the mean of two methods as the independent variable and the difference between two methods as the dependent variable for each of the 40 models as identified by a single observer.

Results

The intraobserver and the interobserver ICC values for the tapered cylinder-based axis and the sphere-based axis were comparable whereas the ICC values for the circle-based axis were lower (Table 1). For all three axes, the ICC values for the internal-external axial angle were greater than those for the varus-valgus angle (Table 1). The ICC values for the internal-external axial angle of the tapered cylinder-based and sphere-based axes indicated good agreement, whereas the ICC values for the varus-valgus angle indicated only moderate agreement. The ICC values for the internal-external axial and varus-valgus angles for the circle-based axis indicated only moderate agreement and fair agreement, respectively.

For the Bland-Altman plots illustrating the agreement between the methods (Figure 6), the limits of agreement were tightest for the comparison between the tapered cylinder-based axis and the sphere-based axis. Even so, the limits of agreement for the internal-external axial

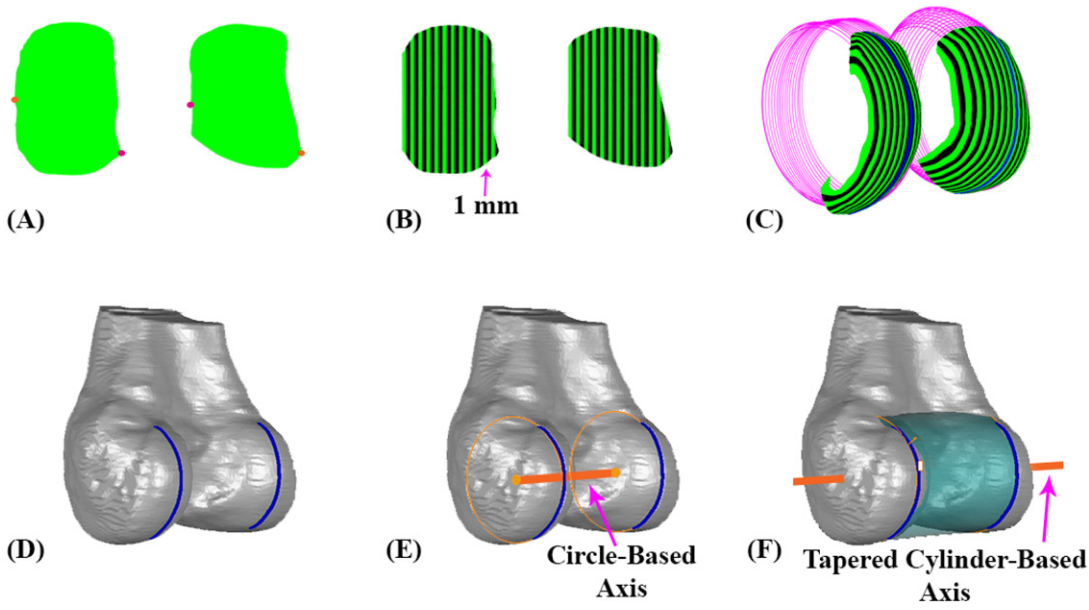

Figure 3. Composite showing a 3D model of a right femur and the methods of computationally obtaining the circle-based and tapered cylinder-based axes. (A) The posterior surface of each femoral condyle was saved as a point cloud and imported to MATLAB. Computationally the most medial and lateral points of the point cloud of each femoral condyle were identified using a routine in MATLAB (Pratt 1987). (B) The space between the most medial and most lateral points of each femoral condyle was filled with 1 mm wide sagittal plane slices. (C) Computationally, a circle was best-fit to each slice of both femoral condyles. The slice with the largest circle was saved for each femoral condyle as a point cloud. (D) The point clouds of the slices with the largest circles were imported into Geomagic. (E) The line connecting the centers of the circles was the circle-based axis. (F) Computationally, a tapered cylinder was best-fit to the point cloud of the two slices with the largest circles. The tapered cylinder-based axis was the axis of the tapered cylinder.

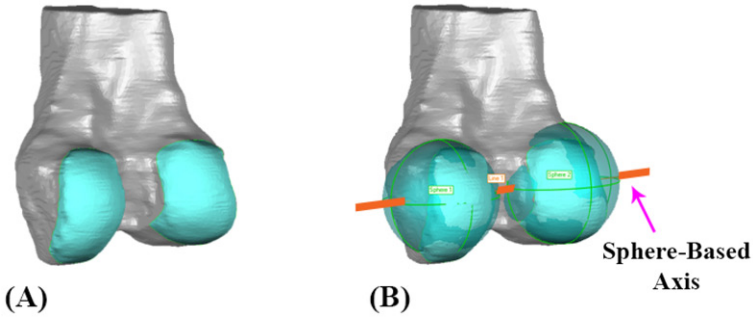

Figure 4. Composite showing a 3D model of a right femur and the method of computationally obtaining the sphere-based axis. (A) The posterior surface of each femoral condyle determined using the methods of Figure 2 was imported into Geomagic. (B) Computationally a sphere was best-fit to each posterior surface. The sphere-based axis connected the centers of the two spheres.

angle were were relatively wide at $+3.6^\circ$ to -3.9° whereas the limits of agreement were tighter at approximately $+1.4^\circ$ to -0.7° for the varus-valgus angle.

Discussion

The present study developed and described three methods for locating the circle-based, tapered cylinder-based and sphere-based axes, determined their repeatability and reproducibility, and assessed their agreement. As indicated by the higher ICC values (Table 1), one key finding was that the repeatability and reproducibility were better for the tapered cylinder-based and sphere-based axes than the circle-based axis. Hence according to these two criteria, the tapered cylinder-based axis and the sphere-based axis offer advantages over the circle-based axis. The lower ICC values for the circle-based axis might have occurred because of the variability introduced by independently fitting circles to each of the medial and lateral condyles in conjunction with basing the circle fit on a 1 mm wide area.

A second key finding was that the limits of agreement were tightest when comparing the

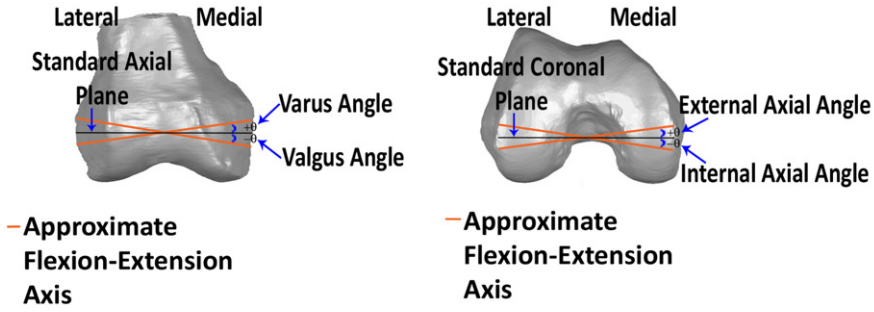

Figure 5. Sign conventions for computing varus-valgus and internal-external axial angles based on the standard planes.

Table 1. Intraobserver (repeatability) and interobserver (reproducibility) intraclass correlation coefficients (ICCs) from two-factor ANOVAs.

	Circle-based axis	Tapered cylinder-based axis	Sphere-based axis
Repeatability			
Internal-external axial angle	0.72	0.81	0.88
Varus-valgus angle	0.47	0.70	0.69
Reproducibility			
Internal-external axial angle	0.50	0.73	0.77
Varus-valgus angle	0.44	0.67	0.61

tapered cylinder-based axis to the sphere-based axis reinforcing the finding from the repeatability-reproducibility analysis that the tapered-cylinder based axis and the sphere-based axis offer advantages over the circle-based axis. However, wide variation in the limits of agreement in the internal-external axial angle relative to the varus-valgus angle was evident (Figure 6). Although the bias was virtually zero for the internal-external axial angle and small at only 0.3° for the varus-valgus angle, nevertheless the wide variation in the limits of agreement for the internal-external axial angle demonstrates that the sphere-based axis is not interchangeable with the tapered cylinder-based axis.

The poor agreement between the sphere-based axis and the tapered cylinder-based axis can be understood by noting that spheres require fitting not only to curvature in the sagittal plane but also to curvature in the coronal plane. However it is the nearly circular curvature in the sagittal plane which forms an effective revolute joint about which FE rotation occurs (Hollister et al. 1993; Churchill et al. 1998; Eckhoff et al. 2003, 2005) and the axis of the revolute is closely approximated by best-fit cylinders with coincident axes (Eckhoff et al. 2003, 2005). Thus, intuitively the tapered cylinder-based axis should be a better approximation of the functional FE axis than the sphere-based axis.

Several methodological issues should be discussed because of their potential to impact our findings. One is the standard planes which served as the basis for computing the varus-valgus and internal-external angles. Focusing on the standard sagittal plane, which was the first standard plane defined (Figure 1), the definition was based on previous research where it has been demonstrated (Hollister et al. 1993) and subsequently independently verified by others (Churchill et al. 1998; Eckhoff et al. 2003) that the functional FE axis of the native tibiofemoral joint is fixed in the femur and hence perpendicular to the plane in which flexion-extension occurs. With the functional FE axis fixed in the femur, an important criterion for a standard sagittal plane is that this plane be closely parallel to the flexion-extension plane. By superimposing the medial and lateral femoral condyles (Figure 1), which are well approximated by circles from about 15° to 115° of flexion (Kurosawa et al. 1985; Iwaki et al. 2000; Asano et al. 2001; Coughlin et al. 2003; Eckhoff et al. 2003; Johal et al. 2005), the standard sagittal plane used herein met this criterion.

Another methodological issue concerns the development of methods for locating the axes. Previous studies that used the circle-based axis (Asano et al. 2001; Coughlin et al. 2003), cylinder-based axis (Eckhoff et al. 2003, 2005; Moro-oka et al. 2008; Matsuki et al. 2017), and sphere-based axis (Kurosawa et al. 1985; Wilson et al. 1998; Victor et al. 2009) did not define the methods with sufficient detail to reproduce the respective methods, which necessitated the present study's development of new methods. It is

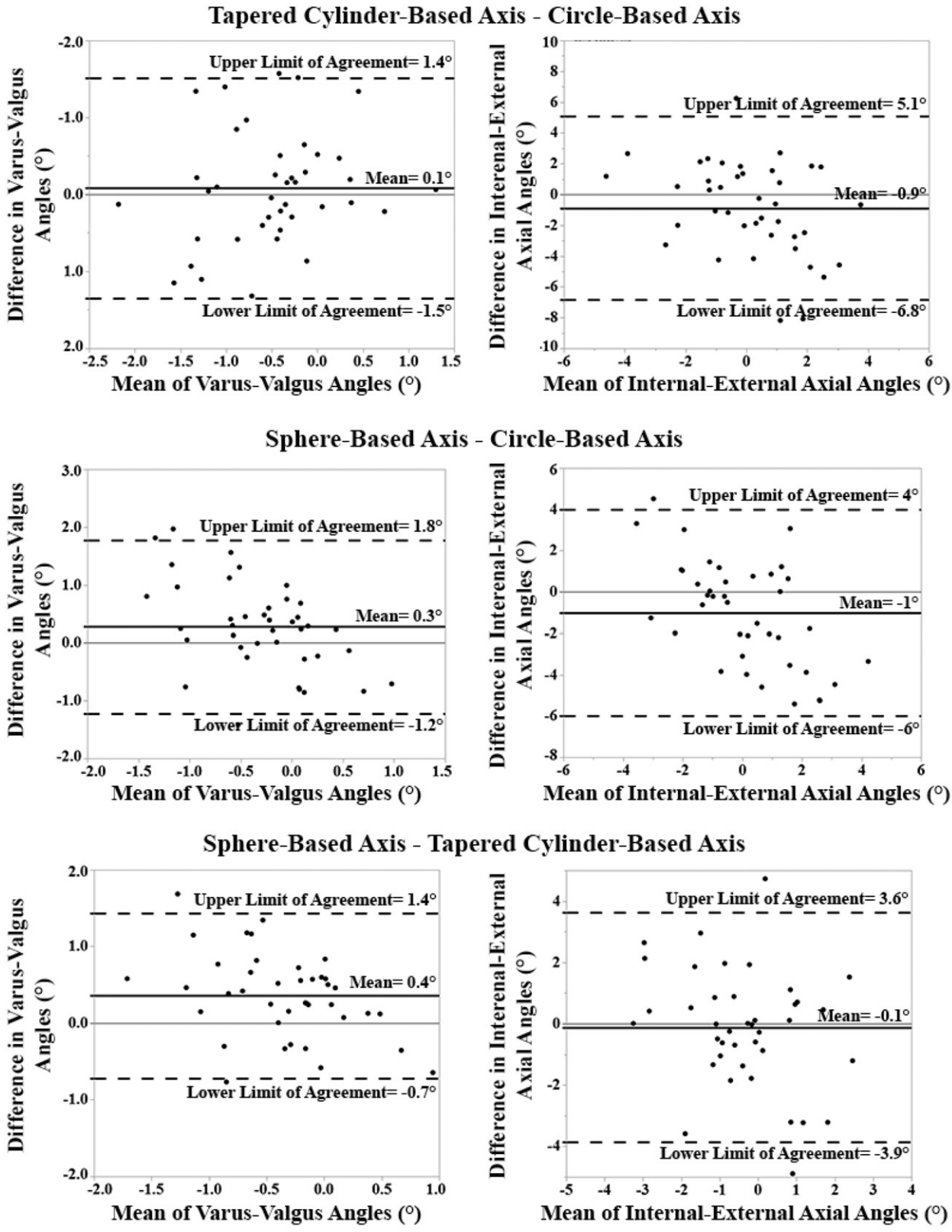

Figure 6. Bland-Altman plots comparing the difference in angles for the three pairs of axes and limits of agreement.

likely that previous studies employed different methods for finding these axes, which might yield different results. However, the method of finding the tapered cylinder-based axis, which was determined computationally in the present study, represented an improvement on the method to find the cylinder-based axis

determined previously since that method determined the axis by manually best fitting two cylinders of slightly different radii to the posterior medial and lateral femoral condyles and imposing the constraint that the axes of the cylinders coincide (Eckhoff et al. 2003, 2005). Fitting a tapered cylinder accounted for the slight difference in radii of the posterior medial and lateral femoral condyles while at the same time enabling a computational best fit of a single object.

A final methodological issue is that the 3D bone models created using MR images obtained from the Osteoarthritis Initiative data base necessarily did not include the articular cartilage. However in native, healthy knees the articular cartilage would be present. The addition of articular cartilage would add a layer to the underlying bone which would amount to increasing the overall size of the femoral condyles. An increase in size of the condyles would not be expected to affect the results in any substantive way.

Conclusions

The repeatability and reproducibility were considerably better for the tapered cylinder-based axis and the sphere-based axis than the circle-based axis indicating the advantages of these axes over the circle-based axis based on these criteria. Further the limits of agreement comparing the sphere-based axis and the tapered cylinder-based axis were tightest. However, the limits of agreement were relatively large for the internal-external axial angle ($+3.6^\circ$ to -3.9°) indicating that the two axes are not in close agreement and hence not interchangeable. Because flexion-extension of the tibio-femoral joint occurs about an axis perpendicular to the sagittal plane, it is the curvature of the condyles in this plane rather than in the coronal plane that controls the motion. Thus, intuitively the tapered cylinder-based axis is preferred over the sphere-based axis when approximating the functional FE axis using 3D bone models of the femur.

Disclosure statement

No potential conflict of interest was reported by the authors.

Funding

The OAI is a public-private partnership comprised of five contracts (N01-AR-2-2258; N01-AR-2-2259; N01-AR-2-2260; N01-AR-2-2261; N01-AR-2-2262) funded by the National Institutes of Health, a branch of the Department of Health and Human Services, and conducted by the OAI Study Investigators. Private funding partners include Merck Research Laboratories; Novartis Pharmaceuticals Corporation, GlaxoSmithKline; and Pfizer, Inc. Private sector funding for the OAI is managed by the Foundation for the National Institutes of Health. This manuscript was prepared using an OAI public use data set and does not necessarily reflect the opinions or views of the OAI investigators, the NIH, or the private funding partners.

References

Asano T, Akagi M, Tanaka K, Tamura J, Nakamura T. 2001. In vivo three-dimensional knee kinematics using a biplanar image-matching technique. Clin Orthop Rel Res. 388:157–166.

Bartlett JW, Frost C. 2008. Reliability, repeatability and reproducibility: analysis of measurement errors in continuous variables. Ultrasound Obstet Gynecol. 31(4): 466–475.

Bland JM, Altman DG. 1986. Statistical methods for assessing agreement between two methods of clinical measurement. Lancet. 1:307–310.

Churchill DL, Incavo SJ, Johnson CC, Beynnon BD. 1998. The transepicondylar axis approximates the optimal flexion axis of the knee. Clin Orthop Rel Res. 356: 111–118.

Coughlin KM, Incavo SJ, Churchill DL, Beynnon BD. 2003. Tibial axis and patellar position relative to the femoral epicondylar axis during squatting. J Arthroplasty. 18(8): 1048–1055.

Eckhoff DG, Bach JM, Spitzer VM, Reinig KD, Bagur MM, Baldini TH, Flannery NM. 2005. Three-dimensional mechanics, kinematics, and morphology of the knee viewed in virtual reality. J Bone Jt Surg. 87-A(Suppl 2): 71–80.

Eckhoff DG, Bach JM, Spitzer VM, Reinig KD, Bagur MM, Baldini TH, Rubinstein D, Humphries S. 2003. Three-dimensional morphology and kinematics of the distal part of the femur viewed in virtual reality. Part II. J Bone Jt Surg. 85-A(Suppl 4):97–104.

Freeman M. 2001. How the knee moves. Curr Orthop. 15(6):444–450.

Grood ES, Suntay WJ. 1983. A joint coordinate system for the clinical description of three-dimensional motions: application to the knee. J Biomech Eng. 105(2):136–144.

Hollister AM, Jatana S, Singh AK, Sullivan WW, Lupichuk AG. 1993. The axes of rotation of the knee. Clin Orthop Rel Res. 290:259–268.

Indrayan A. 2013. Methods of clinical epidemiology. In: Springer series on epidemiology and public health. Berlin, Heidelberg: Springer-Verlag. p. 24.

Iwaki H, Pinskerova V, Freeman MA. 2000. Tibiofemoral movement 1: the shapes and relative movements of the femur and tibia in the unloaded cadaver knee. J Bone Joint Surg. 82-B(8):1189–1195.

Johal P, Williams A, Wragg P, Hunt D, Gedroyc W. 2005. Tibio-femoral movement in the living knee. A study of weight bearing and non-weight bearing knee kinematics using 'interventional' MRI. J Biomech. 38(2):269–276.

Kurosawa H, Walker PS, Abe S, Garg A, Hunter T. 1985. Geometry and motion of the knee for implant and orthotic design. J Biomech. 18(7):487–499.

Matsuki K, Matsuki KO, Kenmoku T, Yamaguchi S, Sasho T, Banks SA. 2017. In vivo kinematics of early-stage osteoarthritic knees during pivot and squat activities. Gait Posture. 58:214–219.

McPherson A, Kärrholm J, Pinskerova V, Sosna A, Martelli S. 2005. Imaging knee position using MRI, RSA/CT and 3D digitisation. J Biomech. 38(2):263–268.

Moro-Oka TA, Hamai S, Miura H, Shimoto T, Higaki H, Fregly BJ, Iwamoto Y, Banks SA. 2008. Dynamic activity dependence of in vivo normal knee kinematics. J Orthop Res. 26(4):428–434.

National Institute of Standards and Technology. 2007. Guidelines for evaluating and expressing the uncertainty of NIST measurement results. http://physics.nist.gov/Pubs/guidelines/contents.

Peterfy CG, Schneider E, Nevitt M. 2008. The osteoarthritis initiative: report on the design rationale for the magnetic resonance imaging protocol for the knee. Osteoarthr Cartil. 16(12):1433–1441.

Piazza SJ, Cavanagh PR. 2000. Measurement of the screw-home motion of the knee is sensitive to errors in axis alignment. J Biomech. 33(8):1029–1034.

Pratt V. 1987. Direct least-squares fitting of algebraic surfaces. Siggraph Comput Graph. 21(4):145–152.

Victor J, Van Doninck D, Labey L, Van Glabbeek F, Parizel P, Bellemans J. 2009. A common reference frame for describing rotation of the distal femur: a CT-based kinematic study using cadavers. J Bone Joint Surg. 91-B(5):683–690.

Wilson DR, Feikes JD, O'Connor JJ. 1998. Ligaments and articular contact guide passive knee flexion. J Biomech. 31(12):1127–1136.

Wilson DR, Feikes JD, Zavatsky AB, O'Connor JJ. 2000. The components of passive knee movement are coupled to flexion angle. J Biomech. 33(4):465–473.

Wu G, Siegler S, Allard P, Kirtley C, Leardini A, Rosenbaum D, Whittle M, D'Lima DD, Cristofolini L, Witte H, et al. 2002. ISB recommendation on definitions of joint coordinate system of various joints for the reporting of human joint motion—part I: ankle, hip, and spine. J Biomech. 35(4):543–548.